Biochimica et Biophysica Acta 1817 (2012) 726–734

Contents lists available at SciVerse ScienceDirect

Biochimica et Biophysica Acta

journal homepage: www.elsevier.com/locate/bbabio

Dynamic water networks in cytochrome *cbb*$_3$ oxidase ☆

Vivek Sharma [a,*], Mårten Wikström [a,*], Ville R.I. Kaila [b,*]

[a] Helsinki Bioenergetics Group, Programme for Structural Biology and Biophysics, Institute of Biotechnology, PB 65 (Viikinkaari 1), University of Helsinki, 00014,Finland
[b] Laboratory of Chemical Physics, National Institute of Diabetes and Digestive and Kidney Diseases, National Institutes of Health, Bethesda, Maryland 20892-0520, USA

ARTICLE INFO

Article history:
Received 13 June 2011
Received in revised form 13 September 2011
Accepted 15 September 2011
Available online 22 September 2011

Keywords:
Proton channel
Proton pumping
cbb$_3$-type cytochrome *c* oxidase
Continuum electrostatics
Density functional theory (DFT)
Molecular dynamics (MD) simulation

ABSTRACT

Heme-copper oxidases (HCOs) are terminal electron acceptors in aerobic respiration. They catalyze the reduction of molecular oxygen to water with concurrent pumping of protons across the mitochondrial and bacterial membranes. Protons required for oxygen reduction chemistry and pumping are transferred through proton uptake channels. Recently, the crystal structure of the first C-type member of the HCO superfamily was resolved [Buschmann et al. Science 329 (2010) 327–330], but crystallographic water molecules could not be identified. Here we have used molecular dynamics (MD) simulations, continuum electrostatic approaches, and quantum chemical cluster calculations to identify proton transfer pathways in cytochrome *cbb*$_3$. In MD simulations we observe formation of stable water chains that connect the highly conserved Glu323 residue on the proximal side of heme b_3 both with the N- and the P-sides of the membrane. We propose that such pathways could be utilized for redox-coupled proton pumping in the C-type oxidases. Electrostatics and quantum chemical calculations suggest an increased proton affinity of Glu323 upon reduction of high-spin heme b_3. Protonation of Glu323 provides a mechanism to tune the redox potential of heme b_3 with possible implications for proton pumping.

1. Introduction

Heme-copper oxidases (HCOs) are terminal enzymes in the respiratory chain of mitochondria and bacteria. HCOs transfer protons across the bacterial plasma membrane and inner mitochondrial membrane, which is coupled to reduction of molecular oxygen to water [1–3]. The electrochemical proton gradient or proton motive force thus formed across the membrane drives the synthesis of ATP by F_oF_1-ATPase [4].

The heme-copper oxidases have been classified into different subfamilies: A-, B-, and C-type [5,6], but also more detailed classification schemes have been suggested [7]. All HCOs comprise a low-spin electron-queuing heme (heme *a*/*b*), and an active site, consisting of a high-spin heme (heme $a_3/b_3/o_3$) and a nearby copper center, Cu_B. Amino acid ligands of the metal centers, *i.e.* five histidines and a cross-linked histidine–tyrosine dimer are also conserved among the A-, B- and C-type HCOs [5–7].

The reduced active site of HCOs binds molecular oxygen to the distal side of the high-spin heme forming an oxygen adduct that may be described as a ferric superoxide species (Fe[III]–$O_2^{*/-}$). This so-called state **A** undergoes subsequent O–O bond scission and formation of the $\mathbf{P_M}$ state (Fe[IV]=O^{2-}, Cu_B[II]–OH^- and a neutral tyrosyl radical). The four electrons and one proton required for the process are taken from the binuclear active site itself; the heme, Cu_B and the cross-linked tyrosine residue [8,9]. In this way the oxidizing potential of dioxygen is transferred to the enzyme as highly oxidizing states of the two metals and the tyrosine. It is the subsequent exergonic reduction of these centers that drives proton translocation, where each proton translocation step is tightly coupled to reduction and protonation of the active site [10].

Despite the wealth of experimental and theoretical studies, particularly on the A-type oxidases, the molecular mechanism of proton-pumping in HCOs is still not fully understood. It has been suggested that the electron-queuing low-spin heme *a* in the A-type oxidases is a critical element in proton-pumping [11–15]. Reduction of the heme results in an increase in proton affinity of a so-called pump- or proton-loading site (PLS), most probably located at or in the vicinity of the A-propionate of the active site heme [10,16–18]. Protonation of the PLS increases the redox-potential of the high-spin heme, which is then reduced by the electron on heme *a*. Reduction of the active site leads to its protonation, which drives out the proton from the PLS to the positively charged side of the membrane (P-side). As the relative position of the hemes and the overall structure of the active site are

Abbreviations: HCO, heme-copper oxidase; MD, molecular dynamics; PLS, proton-loading site; C*c*O, cytochrome *c* oxidase; DFT, density functional theory; C*c*P, cytochrome *c* peroxidase; pT, proton-transfer

☆ All amino acid numbering corresponds to the *cbb*$_3$-type oxidase from *Pseudomonas stutzeri*, unless otherwise mentioned.

* Corresponding authors. Tel.: +358 9 191 59751; fax: +358 9 191 59920.
E-mail addresses: vivek.sharma@helsinki.fi (V. Sharma), marten.wikstrom@helsinki.fi (M. Wikström), ville.kaila@nih.gov (V.R.I. Kaila).

0005-2728/$ – see front matter © 2011 Published by Elsevier B.V.
doi:10.1016/j.bbabio.2011.09.010

conserved structural elements among all HCOs, the general proton-pumping mechanism is believed to be the same [2,3,19, but *cf.* also 20].

The structure of a C-type cytochrome *c* oxidase (C*c*O) from *Pseudomonas stutzeri* was recently solved by X-ray crystallography to 3.2 Å resolution (Fig. 1) [21]. Prior to the structure, biochemical studies and homology modeling approaches identified two distinct features in this enzyme subfamily; a tyrosine residue cross-linked to one of the histidine ligands of Cu_B, analogous to the one found in A- and B-type oxidases, but located in a different helix [5,22–24], and a conserved glutamate residue in the proximal cavity of the active site heme b_3, hydrogen-bonded to the axial histidine ligand of the latter [5,25]. Homology modeling combined with site-directed mutagenesis studies also suggested a proton-channel, analogous in position to the K-channel of A-type oxidases (Fig. 1) [5,26]. Both of these structural elements were observed in the crystal structure. Moreover, recent quantum chemical calculations suggested that the glutamate residue near the proximal histidine ligand of heme b_3 might account for the observed low midpoint potential of the heme as well as for its rhombic EPR spectrum [25,27].

C-type oxidases have a high apparent oxygen affinity (K_M~nM) [28] relative to the A-type oxidases (K_M~μM) [29], which allows the bacteria to survive at low oxygen tensions [28,30]. Based on homology modeling, it was suggested that the different orientation of the cross-linked tyrosine could alter ligand-binding properties of the C-type oxidases [31]. Additionally, crystal structure comparison of A- and C-type oxidases reveal some differences in the heme orientations, which could contribute to

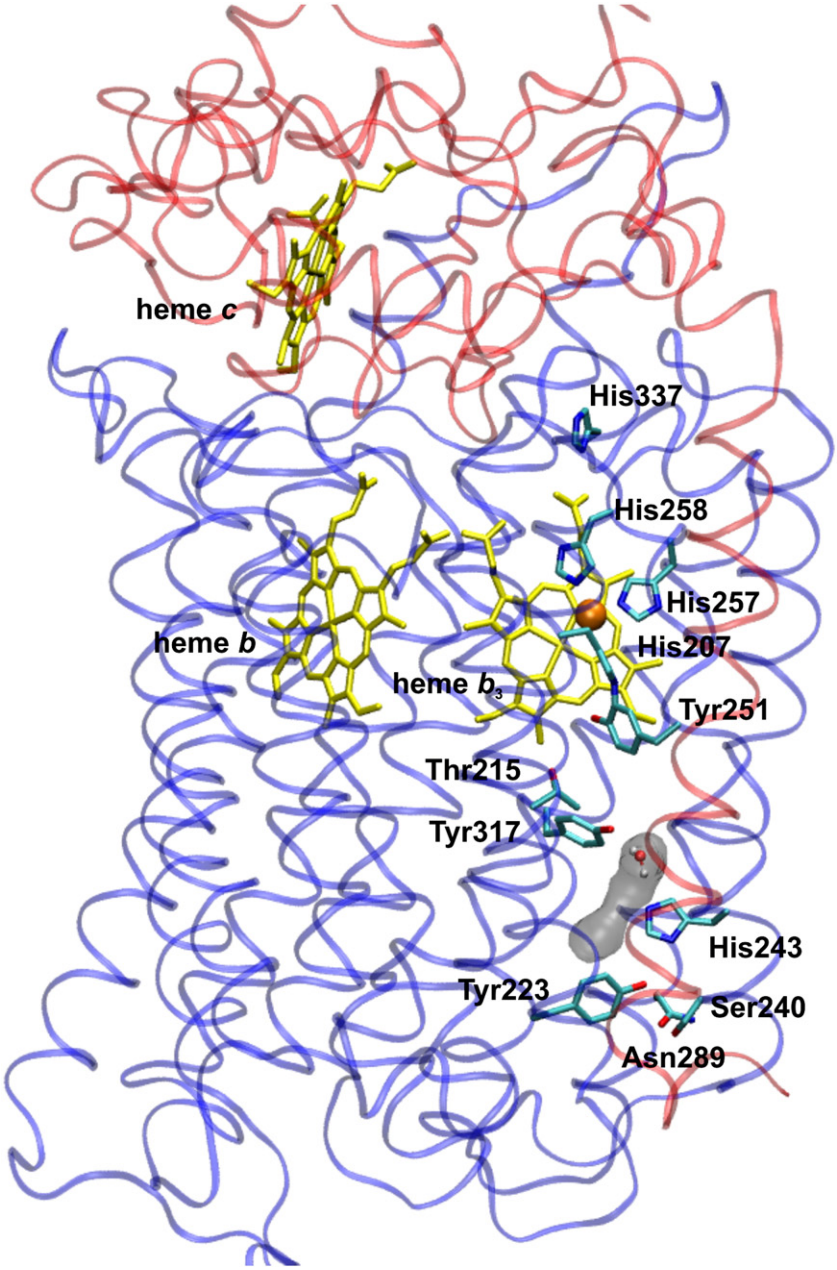

Fig. 1. The subunit NO core-complex of cytochrome cbb_3 oxidase (PDB ID: 3MK7). Subunits N and O are shown with a blue and red ribbon representation, respectively. Heme *c* located in subunit O, and low-spin heme *b* and high-spin heme b_3 located in subunit N are shown in yellow. Cu_B, also located in subunit N, is shown in orange. Conserved amino acid residues around the active site and residues forming a putative proton channel are shown, along with a cavity (gray) containing one modeled water molecule in the vicinity of His243. The figure was prepared using VMD [64].

the high dioxygen affinity of the latter enzymes [21]. Recent quantum chemical calculations suggested that the proximal glutamate might also stabilize a peroxy-intermediate in the oxygen scission process, which is consistent with a low Michaelis constant [32].

C-type oxidases are known to pump protons in whole-cell experiments at a stoichiometry of 1 H^+/e^- [33]. Attempts to reproduce pumping in reconstituted systems have so far yielded only very low stoichiometries [34,35]. Proton pumping requires conduction channels for proton uptake from the N-side of the membrane. In A-type C*c*O two such channels have been identified, the so-called D- and K-channels named after conserved aspartate and lysine residues [36], respectively. Based on site-directed mutagenesis studies in the mitochondrial oxidase from *Bos taurus*, a so-called H-channel has also been suggested to be involved in proton uptake [20]. Protons pumped across the membrane are most probably supplied by the D-channel, while the K-channel is active only in the reductive phase of the catalytic cycle, and transfers two protons to the active site [36,37]. It has recently been suggested that the B-type oxidases, *e.g.* cytochrome ba_3 from *Thermus thermophilus* employs only one channel located at the position analogous to the K-channel in A-type oxidases [38]. Buschmann et al. [21] identified a possible proton uptake channel in the structure of cytochrome cbb_3 at a position analogous to the K-channel in A-type oxidases.

Here we study cytochrome cbb_3 oxidase from *P. stutzeri* using a combination of computational techniques of classical molecular dynamics, continuum electrostatic approaches, and quantum chemical calculations, in order to identify elements involved in proton transfer reactions by the C-type oxidases.

2. Models and methods

2.1. Quantum chemical calculations and derivation of partial charges

Coordinates of redox-active metal sites in subunits N and O; heme *c*, heme *b*, heme b_3 and Cu_B were obtained from the crystal structure of the cbb_3-type cytochrome *c* oxidase from *P. stutzeri* (PDB ID: 3MK7) [21]. Models comprised the metal center and nearby amino acids, shown in Figure S1. Heme b_3 was modeled without a sixth ligand, and with Glu323 both protonated and deprotonated (see also Section 3.3). Cu_B was modeled with a hydroxyl/water as a fourth ligand and Tyr251 protonated. Total charge and spin multiplicity of each model system in both reduced and oxidized states are given in Table S1. The amino acid side chains were terminated at the C_β positions, which were kept fixed during geometry optimization at the BP86 [39,40] level of theory, using the multipole accelerated resolution of identity (MARIJ) approximation [41] and default convergence criteria in TURBOMOLE (energy gradient $= 10^{-6}$ Hartree and geometry gradient $= 10^{-3}$ au) [42]. The def2-SVP [43] basis set was used for all atoms, while metals (Fe/Cu) were treated with a def2-TZVP basis set [44]. After structure optimization, we performed single-point energy calculations at the B3LYP [45,46] level of theory with a def2-TZVP basis set for all atoms, extracting energies and Merz–Kollman partial charges [47]. Single point calculations were also performed using the conductor-like screening model (COSMO) [48] with the dielectric constant set to 4. TURBOMOLE (versions 6.0 and 6.1) [42] was used for all density functional theory (DFT) calculations. The derived partial charges were used in MD simulations and electrostatics calculations (see Sections 2.2 and 2.3). Electrostatic potential (ESP) charges have previously been successfully used in similar calculations [49–53].

Coordinates of optimized geometries of the model systems are available in the supplementary information.

2.2. Molecular dynamics simulations

The NO subunit core complex of cytochrome cbb_3 oxidase (PDB ID: 3MK7) was simulated in redox states: OOOO and OROO, where O and R correspond to the oxidized and reduced state, respectively, and the four letters designate the redox states of heme *c*, heme *b*, heme b_3 and Cu_B, in that order. We predicted protein bound water molecules using the DOWSER program [54], employing different energy cutoffs of −10, −5 and 0 kcal/mol for water insertion. Similar approaches have previously been used to predict water molecules in the A-type C*c*O [55–59], although they are not a rigorous way of computing the free energy of water insertion [60]. Point charges of the metal centers and their protein surroundings obtained from the DFT calculations described above, and the standard CHARMM27 force field [61] supplemented with our in-house developed parameters [49], were used in the MD simulations. Some topology parameters for the heme *c* in subunit O were obtained from the heme parameterization of Autenrieth et al. [62]. All amino acids were kept in their standard protonation states (Asp, Glu — deprotonated, Arg, Lys — protonated, and His, Tyr — neutral) unless otherwise reported. The two-subunit structures of cytochrome cbb_3 were simulated in vacuum for 5 ns after initial energy minimization of 1500 steps and 1 ns of equilibration, using Langevin dynamics (damping coefficient $= 0.1\ ps^{-1}$), at 310 K with a time-step of 1 fs and a 20 Å cutoff for non-bonded interactions. All simulations were performed using NAMD [63]. During the initial 1 ns equilibration the root mean square deviation of the C_α atoms of the protein increased up to ~2.3 Å and remained stable around this value throughout the 5 ns production run from which data was collected for analysis. Data was saved every 0.1 ps, and VMD [64] was used for analysis and visualization of the trajectories. In the analysis of hydrogen-bonded water wires, a hydrogen bond was defined using geometric criteria, with a donor (D)/acceptor (A) distance <3.5 Å and a D–H…A angle >150°.

2.3. Continuum electrostatic calculations

Continuum electrostatic calculations were performed on the NO subunit core complex of cytochrome cbb_3 using the MEAD program [65,66], which solves the Poisson–Boltzmann equation to calculate solvation free energies (pK_a values) of ionizable residues in a protein. The protein interior and membrane slab were modeled using a dielectric constant of 4, while solvent cavities were treated as a high dielectric medium with $\varepsilon = 80$. No explicit water molecules were included in the calculation, except between the propionates of heme b_3 and in the vicinity of His243 (see Section 3.4). All heavy atoms of amino acid residues and cofactors were kept in their crystallographic positions when the positions of added hydrogens were refined with a short energy minimization using NAMD [63]. The calculations were performed in the following redox states: OOOO, OROO, ORORO and ORRR (see Section 2.2), and using the point charges obtained from the DFT calculations. In order to study effects of thermal fluctuations, continuum electrostatic calculations were also performed in the redox states above using an ensemble of 10 structures generated from short (250 ps) MD simulations of the ORRR state. In the electrostatic calculations a water molecule was added as a sixth ligand to the high-spin heme b_3, while a hydroxyl (OH^-) or water (H_2O) molecule was used as the fourth ligand of Cu_B [*cf.* 67]. The standard TIP3P charges [68] were used for the water ligand of heme b_3. The following solution pK_a values were used: Asp (4.5), Glu (4.6), Arg (12.0), Lys (10.4), propionate (4.8), Tyr (9.7), His (6.2 for doubly protonated and 15.0 for singly protonated). The continuum electrostatic calculations yield intrinsic pK_a values, $pK_{a,int}$, for each titratable site and a site–site interaction matrix. The former describes the pK_a of a residue when all other sites are in their neutral state. An actual pK_a value can be obtained, when the $pK_{a,int}$ is combined with the site-site interaction data by Monte-Carlo sampling of 2^N protonation states of the enzyme, where N is the number of titratable residues [65]. The Monte-Carlo sampling was performed using KARLSBERG [69] with default setup values.

3. Results

3.1. Water prediction

Protein-bound water molecules can be predicted using an interaction energy criterion between the water molecule and the protein surroundings [54,70]. The water prediction software DOWSER [54] and related computer programs [57,70], predict a water molecule inside the protein if its interaction energy with the protein is below a given energy threshold. The structure of cbb_3-oxidase [21] was simulated in the ORRR redox state using three different energy cutoffs of 0, −5, and −10 kcal/mol, followed by subsequent MD simulations in different redox states (OOOO and OROO). We observe $N = 163$, 139 and 97 water molecules using these cutoff values, respectively, with minimal changes in water occupancy with the change of redox state. More sophisticated force field based calculation of these water-protein interaction energies using NAMD yield a high van der Waals energy for some of the predicted water molecules obtained with the large energy cutoff in DOWSER. However, upon subsequent energy minimization the energy relaxes to lower values of $\sim -19 \pm 7$ kcal/mol, which is consistent with previous similar water insertion estimates [58]. It is observed that during MD simulations the interaction energy fluctuates around this value as water molecules move between different sites.

Analysis of the water-loaded structure shows a population of water molecules at the location of the 'canonical' K-channel. $N = 4$, 7 and 10 water molecules are predicted using the energy cutoffs of −10, −5 and 0 kcal/mol, respectively. Stable water molecules are predicted near Tyr317 and the proximal Glu323, which subsequently take part in formation of a water chain (see Section 3.2). An extended cavity is observed between the distal and proximal sides of high-spin heme b_3 (His345/Glu323 site, Fig. 2). This cavity comprises water molecules, *e.g.* W97, which escape to other regions of the protein during the simulation (see Section 3.2). Thus, in analogy to A-type oxidases, water molecules that are produced during turnover may be utilized for proton transfer also in C-type oxidases [55,56,71].

3.2. Proton pathways

Molecular dynamics simulations on the water-loaded subunit NO complex, with a 0 kcal/mol energy cutoff for the water insertion threshold, suggest that reduction of the low-spin heme *b* (state OROO) leads to formation of a Y-shaped, bifurcated water wire. One branch appears in the same structural position as the 'canonical' K-pathway (see Section 1), connecting the N-side of the membrane to the cross-linked tyrosine in the active site (Fig. 3C), and the other leads to the proximal side of heme b_3 (Fig. 3A). The water wire begins at the conserved residues Asn289 and Ser240, located near the N-side, and connects to the highly conserved Tyr317 that acts as the bifurcation point (Fig. 3A and C). The branch to the proximal side of heme b_3 leads to the conserved Glu323 via two polar residues, Ser320 and Thr321 (Fig. 3A). Out of five independent 5 ns MD simulations in the OROO redox state, three simulations show stable hydrogen-bonded connectivity between Tyr317 and Glu323, supporting a possible role of Ser320 and water molecules in the proton uptake. To estimate the stability of the pathway shown in Fig. 3A, we calculated the occupancies of hydrogen bonds within these water molecules and protein residues, as well as the probability of a continuous hydrogen-bonded water-chain from Tyr317 to Glu323 (Table 1). With nearly 50% occupancy for many individual hydrogen bonds, we also obtain a total chain persistence probability of *ca.* 10%. At ambient conditions, this

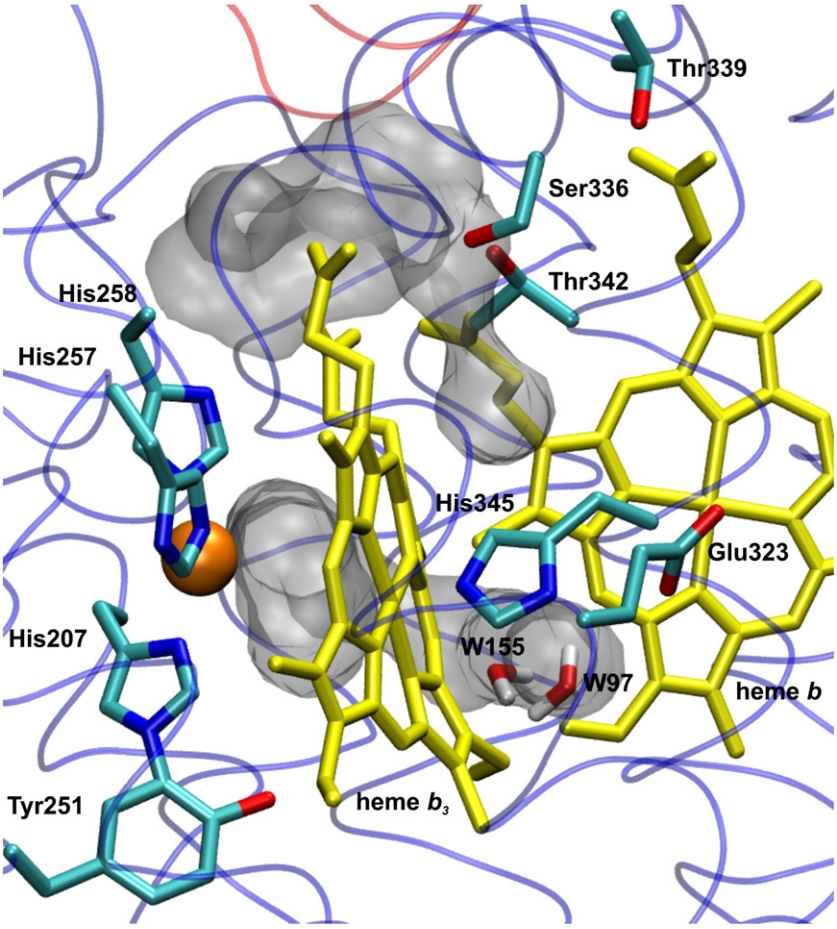

Fig. 2. Cavities around high-spin heme b_3 are shown as gray surfaces. Computationally predicted water molecules are marked with prefix W. The figure was prepared using VMD [64].

would be sufficient for an overall stepwise proton transfer process, and even fast semi-concerted proton transfer over shorter cluster pairs along such a "wire" [3,72].

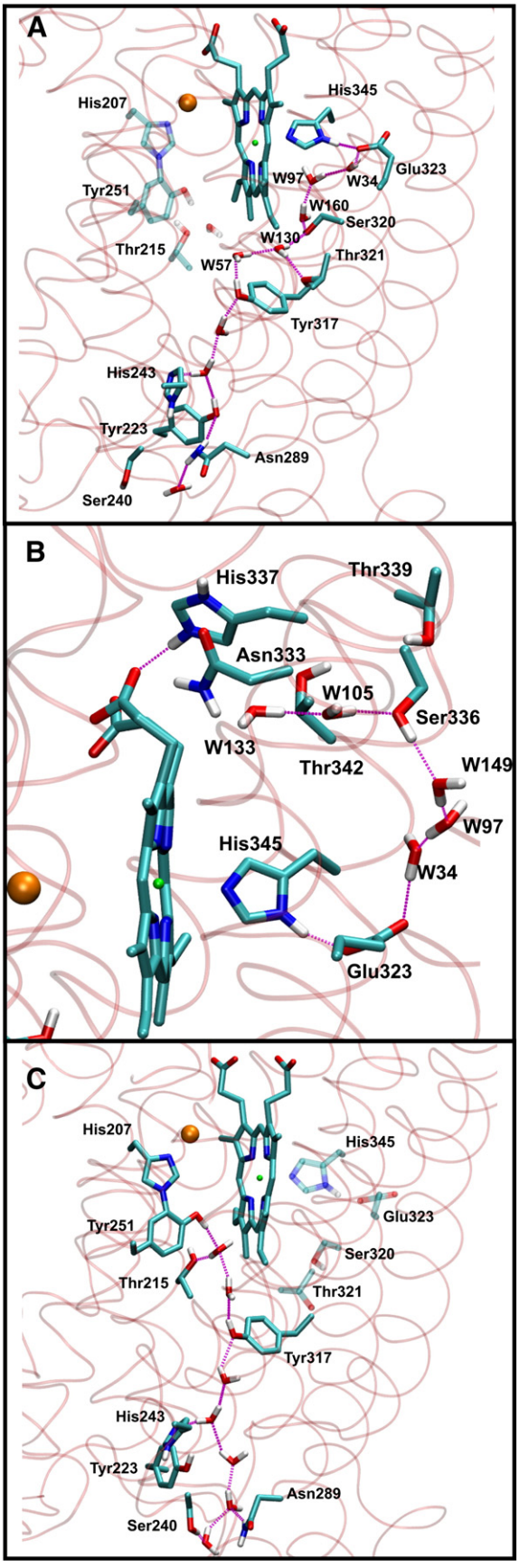

Table 1
Occupancy (%) of the selected hydrogen bonds and probability (%) of a continuous water-chain obtained from 5 ns long MD runs. The analysis was performed using VMD [64].

Tyr317 → Glu323[a,f]	Occ. (%)	Glu323 → His337[b,f]	Occ. (%)	Tyr317 → Glu323[c,f]	Occ. (%)
Tyr317-W57	55	W34-Glu323	71	Tyr317-W29	25
W57-W160	33	W133-W105	82	W29-W57	55
W57-W130	60	W133-Ser336	36	W57-W97	47
W160-Ser320	47	W149-Glu323	38	W97-Ser320	56
W97-Ser320	34	W133-His337	37	Ser320-W102	41
W97-W34	55	W105-Ser336	24	W102-W155	40
W34-Glu323	78	W105-His337	45	W155-W149	68
W160-W97	24	W97-W34	28	W149-W34	41
		W97-W149	11	W34-Glu323	82
				W57-Tyr317	36
Water-chain[d,g] persistence	10	Water-chain[e,g] persistence	15		

[a] Occupations computed from MD simulation in state OROO corresponding to a water configuration shown in Fig. 3A.
[b] Occupations computed from MD simulation in state OROO corresponding to a water configuration shown in Fig. 3B.
[c] Occupations computed from MD simulation in state OOOO corresponding to a water configuration shown in Fig. 3A.
[d] Probability (%) of the continuous water-chain from Tyr317 → Glu323 (Fig. 3A).
[e] Probability (%) of the continuous water-chain from Glu323 → His337 (Fig. 3B).
[f] Occupancy of the hydrogen bond is calculated by counting the number of frames in which it remains formed divided by the total frames used. Hydrogen bond criterion given in Section 2.2 is used.
[g] Probability (%) corresponds to the number of frames in which the water-chain remains fully connected, divided by the total number of frames used for analysis. Hydrogen bond criterion given in Section 2.2 is used.

In the two other simulations another water chain forms between Glu323 and the A-propionate region of heme b_3, connecting the sites through the highly conserved polar residue Ser336 with an array of water molecules (Fig. 3B). The occupancies of selected hydrogen bonds in this route and the probability of continuous chain persistence are also given in Table 1, indicating effective proton conducting properties. The total chain persistence probabilities from Tyr317 to Glu323 and Glu323 to His337 of *ca.* 10–15% are also consistent with previous estimates of similar chain lengths [57].

We note that the water molecules predicted in the extended cavity (*e.g.* W97 in Fig. 2), take part in water wire formation (W97 in Fig. 3A and B). We also observe that some of the water molecules (W57 and W34) involved in the water chains shown in Fig. 3A and B were originally predicted to be near Glu323 and Tyr317. In the five independent MD simulations, the water molecules involved in the water chains change their identity, and the hydrogen bonds between water molecules and protein residues fluctuate, thus making it difficult to quantitatively assess the stability of the water wires. However, the data shown in Table 1 clearly indicate that the water chains remain dynamically stable over nanosecond timescales once formed. The two observed water chains combined (Fig. 3A and B) suggest unique proton transfer (pT) routes that may be used for redox-coupled proton pumping in C-type oxidases.

The water chains between Tyr317 and Glu323, and between Glu323 and the A-propionate region of heme b_3, do not form in simulations where the DOWSER energy cutoff for water insertion is decreased to −5 kcal/mol or lower. In such simulations, the water molecules move elsewhere in the protein to patch empty protein cavities. However, as previously discussed [56,73,74], it remains likely that the proton conducting water molecules in HCO may have a high conformational

Fig. 3. Hydrogen-bonded water chains in C-type oxidases obtained from MD simulations. The water chains connect A) the N-side with proximal glutamate (Glu323) and, B) the proximal glutamate with the A-propionate region, with possible importance for pumping. C) Water chains connecting the N-side with the active site of oxygen reduction. The bifurcation point at Tyr317 is located below heme b_3. Only hydrogen atoms connected to oxygen and nitrogen are shown. Water molecules are marked with a W prefix. The figure was prepared using VMD [64].

entropy and thermodynamic instability in order to avoid accumulation of internal pressure in the protein cavities during turnover.

Five independent 5 ns MD simulations were also performed in the fully oxidized state (OOOO). Interestingly, the branch leading from Glu323 to the A-propionate region of heme b_3 is not observed in such simulations, while in one of the five simulations we observe a stable pathway between Tyr317 and Glu323. The occupancies of selected hydrogen bonds in these simulations are also given in Table 1. The data suggest that an electron on heme *b* (state OROO) stabilizes the water chains on the proximal side of heme b_3 (Fig. 3A and B).

3.3. Protonation states of Glu323 and His337

Glu323 is hydrogen-bonded to the proximal histidine ligand of heme b_3, and is a unique feature of the C-type oxidases, absent in the A- and B-type subfamilies. Analogous His-Asp motifs are also present in other heme enzymes, *e.g.* cytochrome *c* peroxidase (C*c*P) [75]. Based on the results from the MD simulations discussed above, Glu323 seems to form part of a water wire that might be involved in proton translocation. Hence this residue is likely to become reversibly protonated during turnover. Indeed, our continuum electrostatic calculations predict protonation of Glu323 upon reduction of the high-spin heme b_3 ($pK_a > 10$), while it may or may not be protonated when heme b_3 is oxidized ($pK_a \sim 7$) (Table 2). The table also reports pK_a values obtained using an ensemble of structures obtained from short MD simulations, suggesting a similar trend but a smaller increase in proton affinity upon reduction of the heme b_3. A very strong redox state dependent pK_a-shift is predicted by the DFT calculations, in which reduction of heme b_3 stabilizes the protonated glutamic acid by 16 kcal/mol (~11 pK-units) at $\varepsilon = 4$. The large magnitude of this quantum-chemically determined pK_a-shift may be due to the small cluster models used here, and illustrates the challenges in estimating pK_a values by classical approaches; nonetheless these calculations support an increased protonation probability of the proximal Glu323 upon heme reduction.

His337 is a highly conserved residue in the C-type oxidases [5,6] (Fig. 1), forming a hydrogen bond to the A-propionate of heme b_3. In A-type oxidases the analogous histidine also ligates to a Mg^{2+}-ion, while in B-type oxidases it donates a hydrogen bond to a glutamate residue from subunit II [76]. In contrast, in the structure of cytochrome cbb_3, His337 has no interaction partners besides the A-propionate, which results in a very high computed pK_a (>14) in all redox-states studied here (Table 2). The doubly protonated histidine thus effectively neutralizes the negative charge of the A-propionate. Based on suggestions for the A-type oxidases [18,77], His337 might together with the A-propionate of heme b_3 form part of the so-called proton-loading site (PLS) of the proton pump mechanism (see Section 1). The present pK_a calculations predict deprotonated heme b_3 propionates in all redox states studied here (Table 2), as was previously found for the A-type oxidases [67,78]. However, as recently observed in combined MD and electrostatic studies of cytochrome aa_3 from *Bos taurus*, redox-state driven conformational changes at the A-propionate might increase the proton affinity of the propionates considerably [18].

Table 2
Acid constants (pK_a values) or protonation states of selected residues in different redox states obtained from continuum electrostatics simulations using the X-ray structure (first value) or an ensemble of structures obtained from MD simulations (second value, see Section 2.3 for discussion).

Residue	OOOO	OROO	OROR	ORRR
His257[a]	P[c]	P	P	P
His258[a]	P	P	P	P
Tyr251	P	P	P	P
His337[b]	P	P	P	P
His345[a]	P	P	P	P
Glu323	6.4/6.1	6.7/6.4	6.0/5.0	10.7/7.3
His243[b]	D[d]	D	D	D
PrpA *a*	D	D	D	D
PrpD *a*	D	D	D	D
PrpA a_3	D	D	D	D
PrpD a_3	D	1.1/D	D	3.2/D
Glu122	D	D	D	D
Glu125	D	D	D	D

[a] Modeled as imidazole ↔ imidazolate.
[b] Modeled as imidazole ↔ imidazolium.
[c] P: protonated ($pK_a > 14$).
[d] D: deprotonated ($pK_a < 0$).

3.4. K-channel

We observe that a proton transfer pathway forms at a location analogous to the 'canonical' K-channel, and is stable for nanoseconds irrespective of the redox state of the heme groups, or the different energy cutoffs used for water prediction (Fig. 3C). The probability for a continuous water-chain between Asn289 and Tyr251 (Fig. 3C) is ca. 2.5%, as obtained from a 5 ns production run in the OOOO redox state. The reason for this somewhat lower chain persistence probability, relative to 10–15% observed for chains between Glu323 and Tyr317/His337, is most likely due the longer chain length. Homology modeling, biochemical experiments, and X-ray data suggest the presence of a proton channel in this location, corroborating the current MD simulation data. The hydrogen-bonded network comprises residues Ser240, Asn289, Tyr223, His243, Tyr317 and water molecules connecting the N-side to the active site through the cross-linked Tyr251 (Fig. 3C), or to the proximal Glu323 via Ser320 and Thr321 (Fig. 3A). Many of these residues have been mutated and suggested to be involved in proton uptake from the N-side [26]. However, the role of the well-conserved His243 residue in proton uptake has remained controversial: its mutation to glycine in cytochrome cbb_3 from *Rhodobacter sphaeroides*, and to valine in the *Bradyrhizobium japonicum* enzyme resulted in decreased catalytic activity [26,79], but its mutation to alanine in the *R. sphaeroides* enzyme yields wild-type activity [80].

Continuum electrostatic calculations suggest that His243 is neutral in all studied redox states (Table 2). The proton affinity remains nearly unaltered even when an explicit water molecule is modeled near this residue with His243 protonated and the water-histidine interactions minimized (Fig. 1 and Table 2). In the MD simulations we observe that the hydrogen-bonded network bypasses His243 in many configurations, following a pathway involving a water molecule located in the cavity adjacent to this residue (Fig. 1, Fig. 3A and C). This could allow pT without protonation/deprotonation of His243, even though this residue clearly has a stabilizing effect on the observed water wire (Fig. 3A and C).

3.5. Other possible water-filled cavities

Large energy cutoffs in water insertion calculations have previously been used to identify sites of water molecules in the interior of C*c*O [56–58], together with statistical mechanical approaches [71,81]. Simple interaction energy approaches using high energy cutoffs, might lead to formation of artificial internal pressure within protein cavities. When a cutoff of 0 kcal/mol is used in the DOWSER calculations, 163 water molecules are found in the two-subunit enzyme. In such conditions a water-filled cavity is observed in the region analogous to the D-channel in A-type oxidases. However, due to two hydrophobic blockages in the region it has been suggested not to conduct protons [21]. In some simulations we observe conformational changes in these hydrophobic residues, allowing a transient water chain that connects residues Thr84, Ser77, Tyr141, Asn161 and Tyr205 (Fig. 4). This pathway leads up to the P-side of the membrane, near two conserved glutamates (Glu122 and Glu125), and the propionates of the low-spin heme *b*. Mutation of Glu122 to glutamine in cbb_3 oxidase from *Vibrio cholerae* abolished activity almost completely [26]. Similar results were obtained when this residue, which is a ligand of the Ca^{+2} ion near the D-propionate

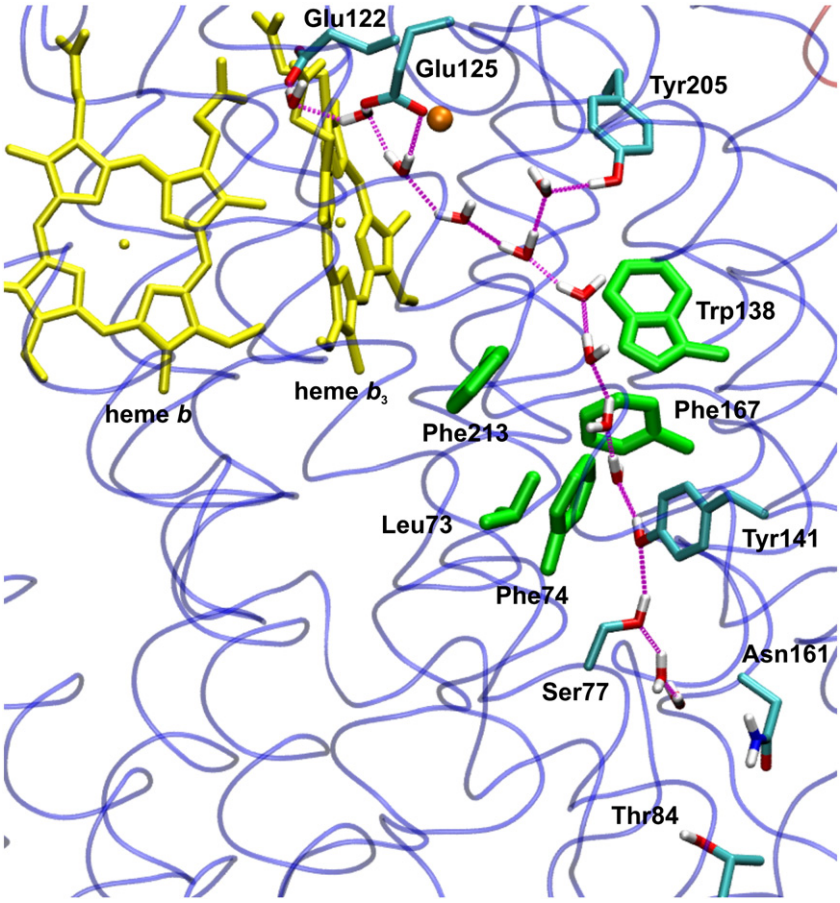

Fig. 4. Transient water networks predicted at a location analogous to the D-channel region in A-type oxidases. The disrupted hydrophobic block formed by non-polar residues, Leu73, Phe74, Trp138, Phe167, Phe213, is shown in green. Only hydrogen atoms attached to oxygen and nitrogen are shown. The figure was prepared with VMD [64].

of heme b_3, was mutated to glycine in the *R. sphaeroides* enzyme [26]. In contrast, analogous mutations of Glu125 retain significant activity [26]. Neither of these glutamates becomes protonated in the present electrostatic calculations (Table 2). Moreover, the tyrosine analogous to Tyr205 (Fig. 4) has been mutated to phenylalanine in the *R. sphaeroides* enzyme with virtually no effect on activity or proton pumping [5]. We conclude that neither glutamate residue seems to be important for proton transfer, suggesting that the transiently observed "D-like" pathway is an artifact of the high energy cutoff used in prediction of water molecules.

4. Discussion

4.1. Functionally critical residues

MD simulations of cytochrome cbb_3 with computationally inserted water molecules in the redox state OROO show formation of a bifurcated proton transfer pathway from the N-side of the membrane, where one branch leads to the binuclear center (mimicking the K-pathway in the A-type oxidases), and the other reaches Glu323 on the proximal side of heme b_3 (Fig. 3A). Simulations in the same redox state show further formation of a water chain between the proximal Glu323 and the A-propionate region of heme b_3 (Fig. 3B). These two pathways (Tyr317 → Glu323 and Glu323 → His337/A-propionate) could be involved in the proton pumping machinery in C-type oxidases. Tyr317 appears to form the bifurcation point from where protons are donated either to the active site for oxygen reduction chemistry, or to the proximal side of heme b_3 for pumping (Fig. 3A). The importance of Tyr317 as a bifurcation point is consistent with mutational experiments [26], where replacement of this residue with phenylalanine in cytochrome cbb_3 from *V. cholerae*, or with glycine in the *R. sphaeroides* enzyme, yielded negligible activity.

Water molecules and two polar residues (Ser320 and Thr321) are found further up along the pathway towards Glu323 (Fig. 3A). We note that Ser320 is a highly conserved residue in the C-type oxidases, even though it is replaced by alanine in some of the sequences. Based on MD simulations, Glu323 can connect both to the N-side (Fig. 3A) and the P-side (Fig. 3B) through water chains and conserved polar residues, suggesting that it could become protonated from the N-side and release its proton to the P-side. If this is part of the proton-pumping mechanism it imposes immediate questions of how proton leaks are prevented, since continuous connectivity to both sides abolishes proton-pumping activity [82,83]. Continuum electrostatic calculations and small quantum chemical cluster models suggest protonation of Glu323 upon reduction of heme b_3, which might drive the pumping process. Redox-state driven protonation of Glu323 is consistent with redox titrations of heme b_3 where a relatively strong pH-dependence of the midpoint redox potential is observed, even when heme b and Cu_B are reduced [25]. This is in contrast to the hemes in the A-type oxidases, which have a very weak pH dependence when the companion heme is reduced [84]. A similar redox-dependent protonation event of the proximal aspartate has been suggested in CcP, based on analysis of the dependence of the midpoint redox potential on pH [75].

The putative proton transfer pathway from Glu323 towards the A-propionate region of heme b_3 comprises a cavity lined with polar residues, Ser336, Thr342 and Thr339 (Fig. 2). MD simulations suggest a critical role of Ser336 in proton transfer from Glu323 to the His337/A-propionate region (Fig. 3B). Their importance in proton transfer could be assessed by mutating these polar residues to non-

polar residues. Thr339 has already been mutated to alanine in cytochrome cbb_3 from *Rhodobacter capsulatus* yielding 44% of wild-type activity [85], suggesting that it may have a role in proton transfer through this route. However, according to our MD simulations, the side chain of Thr339 points into the hydrophilic interface between subunits N and O, and may thus be less important for proton transfer, while the two other polar residues, Ser336 and Thr342, appear to be stronger candidates to be tested.

4.2. A possible scenario of proton pumping

In the fully oxidized state, the His345/Glu323 pair is likely to share a single proton. Based on electrostatic calculations (Table 2), His345 is neutral and Glu323 is deprotonated. The net negative charge in the region is expected to be responsible for the observed low redox potential of high-spin heme b_3 [25]. Upon reduction of the low-spin heme *b* (OROO), we observed formation of water arrays from the N-side of the membrane to the proximal Glu323 and also between Glu323 and the A-propionate region of heme b_3 (Fig. 3A and B). These water chains may carry the proton to the A-propionate of heme b_3, by analogy to what has been suggested in the A-type oxidases [10,74], where reduction of low-spin heme *a* is coupled to protonation of the PLS from the D-channel [3,10,15]. Systematic redox-state dependent conformational changes in the region of the A-propionate of heme a_3 as recently observed in A-type oxidases [18,77], are possible in the C-type oxidases, and will be subject of further studies. The immediate proton donor for loading the PLS in the putative proton pump pathway suggested here is likely to be Tyr317, which is analogous to what has recently been suggested in the A-type oxidase. In the latter, a conserved tyrosine in the D-channel (Tyr35 *Paracoccus denitrificans* numbering) donates a proton to the PLS via a conserved glutamic acid (Glu278 *P. denitrificans* numbering) [86].

Protonation of the A-propionate of heme b_3 is expected to increase the redox-potential of heme b_3. However, due to its low "ground state" redox potential, the rate and extent of electron transfer from the neighboring heme may be low. Subsequent protonation of Glu323 from the N-side is however expected to further increase the midpoint potential of heme b_3, increasing the rate and extent of inter-heme electron transfer. Redox titrations of heme b_3 indeed suggest a relatively strong pH dependence [25]. Reduction of heme b_3 is expected to increase the proton affinity of the oxygenous ligand at the distal side, which would accept a "substrate proton" from Tyr317 via the cross-linked Tyr251. Due to charge cancelation, the electrostatic attraction between the redox electron and the "pumped" proton in the PLS would be lost, leading to its ejection to the P-side of the membrane.

Supplementary materials related to this article can be found online at doi:10.1016/j.bbabio.2011.09.010.

Acknowledgements

V. S. is supported from Sigrid Jusélius Foundation and Viikki Graduate School in Molecular Biosciences. V.R.I.K. acknowledges the European Molecular Biology Organization (EMBO) for a Long-Term Fellowship and the Intramural Research Program of the National Institutes of Health, National Institute of Diabetes and Digestive and Kidney Diseases for support. The research was supported by the Sigrid Jusélius Foundation, Biocentrum Helsinki and the Academy of Finland. The Center for Scientific Computing (CSC), Finland, and the Biowulf cluster at NIH are acknowledged for computing time.

References

[1] M.K.F. Wikström, Proton pump coupled to cytochrome *c* oxidase in mitochondria, Nature 266 (1977) 271–273.
[2] S. Ferguson-Miller, G.T. Babcock, Heme copper terminal oxidases, Chem. Rev. 96 (1996) 2889–2908.
[3] V.R.I. Kaila, M.I. Verkhovsky, M. Wikström, Proton-coupled electron transfer in cytochrome oxidase, Chem. Rev. 110 (2010) 7062–7081.
[4] M. Yoshida, E. Muneyuki, T. Hisabori, ATP synthase — a marvellous rotary engine of the cell, Nat. Rev. Mol. Cell Biol. 2 (2001) 669–677.
[5] V. Sharma, A. Puustinen, M. Wikström, L. Laakkonen, Sequence analysis of the cbb_3 oxidases and an atomic model for the *Rhodobacter sphaeroides* enzyme, Biochemistry 45 (2006) 5754–5765.
[6] M.M. Pereira, M. Santana, M. Teixeira, A novel scenario for the evolution of haem-copper oxygen reductases, Biochim. Biophys. Acta 1505 (2001) 185–208.
[7] J. Hemp, R.B. Gennis, Diversity of the heme-copper superfamily in Archaea: insights from genomics and structural modeling, Results Probl. Cell Differ. 45 (2008) 1–31.
[8] D.A. Proshlyakov, M.A. Pressier, C. DeMaso, J.F. Leykam, D.L. DeWitt, G.T. Babcock, Oxygen activation and reduction in respiration: involvement of redox-active tyrosine 244, Science 290 (2000) 1588–1591.
[9] E.A. Gorbikova, I. Belevich, M. Wikström, M.I. Verkhovsky, The proton donor for O—O bond scission by cytochrome *c* oxidase, Proc. Natl. Acad. Sci. U. S. A. 105 (2008) 10733–10737.
[10] M. Wikström, M.I. Verkhovsky, Mechanism and energetics of proton translocation by the respiratory heme-copper oxidases, Biochim. Biophys. Acta 1767 (2007) 1200–1214.
[11] G. Capitanio, P.L. Martino, N. Capitanio, S. Papa, Redox Bohr effects and the role of heme a in the proton pump of bovine heart cytochrome c oxidase, Biochim. Biophys. Acta 1807 (2011) 1287–1294.
[12] V.Y. Artzatbanov, A.A. Konstantinov, V.P. Skulachev, Involvement of intramitochondrial protons in redox reactions of cytochrome *a*, FEBS Lett. 87 (1978) 180–185.
[13] H. Michel, Cytochrome *c* oxidase: catalytic cycle and mechanisms of proton pump — a discussion, Biochemistry 38 (1999) 15129–15140.
[14] T. Tsukihara, K. Shimokata, Y. Katayama, H. Shimada, K. Muramoto, H. Aoyama, M. Mochizuki, K. Shinzawa-Itoh, E. Yamashita, M. Yao, Y. Ishimura, S. Yoshikawa, The low-spin heme of cytochrome *c* oxidase as the driving element of the proton-pumping process, Proc. Natl. Acad. Sci. U. S. A. 100 (2003) 15304–15309.
[15] I. Belevich, D.A. Bloch, N. Belevich, M. Wikström, M.I. Verkhovsky, Exploring the proton pump mechanism of cytochrome *c* oxidase in real time, Proc. Natl. Acad. Sci. U. S. A. 104 (2007) 2685–2690.
[16] P.E.M. Siegbahn, M.R.A. Blomberg, Energy diagrams and mechanism for proton pumping in cytochrome *c* oxidase, Biochim. Biophys. Acta 1767 (2007) 1143–1156.
[17] R. Sugitani, E.S. Medvedev, A.A. Stuchebrukhov, Theoretical and computational analysis of the membrane potential generated by cytochrome *c* oxidase upon single electron injection into the enzyme, Biochim. Biophys. Acta 1777 (2008) 1129–1139.
[18] V.R.I. Kaila, V. Sharma, M. Wikström, The identity of the transient proton loading site of the proton-pumping mechanism of cytochrome *c* oxidase, Biochim. Biophys. Acta 1807 (2011) 80–84.
[19] P. Brzezinski, P. Ädelroth, Design principles of proton-pumping haem-copper oxidases, Curr. Opin. Struct. Biol. 16 (2006) 465–472.
[20] K. Shimokata, Y. Katayama, H. Murayama, M. Suematsu, T. Tsukihara, K. Muramoto, H. Aoyama, S. Yoshikawa, H. Shimada, The proton pumping pathway of bovine heart cytochrome *c* oxidase, Proc. Natl. Acad. Sci. U. S. A. 104 (2007) 4200–4205.
[21] S. Buschmann, E. Warkentin, H. Xie, J.D. Langer, U. Ermler, H. Michel, The structure of cbb_3 cytochrome oxidase provides insights into proton pumping, Science 329 (2010) 327–330.
[22] J. Hemp, C. Christian, B. Barquera, R.B. Gennis, T.J. Martinez, Helix switching of a key active-site residue in the cytochrome cbb_3 oxidases, Biochemistry 44 (2005) 10766–10775.
[23] V. Rauhamäki, M. Baumann, R. Soliymani, A. Puustinen, M. Wikström, Identification of a histidine-tyrosine cross-link in the active site of the cbb_3-type cytochrome *c* oxidase from *Rhodobacter sphaeroides*, Proc. Natl. Acad. Sci. U. S. A. 103 (2006) 16135–16140.
[24] J. Hemp, D.E. Robinson, K.B. Ganesan, T.J. Martinez, N.L. Kelleher, R.B. Gennis, Evolutionary migration of a post-translationally modified active-site residue in the proton-pumping heme-copper oxygen reductases, Biochemistry 45 (2006) 15405–15410.
[25] V. Rauhamäki, D.A. Bloch, M.I. Verkhovsky, M. Wikström, Active site of cytochrome cbb_3, J. Biol. Chem. 284 (2009) 11301–11308.
[26] J. Hemp, H. Han, J.H. Roh, S. Kaplan, T.J. Martinez, R.B. Gennis, Comparative genomics and site-directed mutagenesis support the existence of only one input channel for protons in the C-family (cbb_3 oxidase) of heme-copper oxygen reductases, Biochemistry 46 (2007) 9963–9972.
[27] V. Sharma, M. Wikström, V.R.I. Kaila, Redox-coupled proton transfer in the active site of cytochrome cbb_3, Biochim. Biophys. Acta 1797 (2010) 1512–1520.
[28] O. Preisig, R. Zufferey, L. Thöny-Meyer, C.A. Appleby, H. Hennecke, A high-affinity cbb_3 type cytochrome oxidase terminates the symbiosis-specific respiratory chain of *Bradyrhizobium japonicum*, J. Bacteriol. 178 (1996) 1532–1538.
[29] S. Massari, A. Bösel, J.M. Wrigglesworth, The variation of Km for oxygen of cytochrome oxidase with turnover under de-energized and energized conditions, Biochem. Soc. Trans. 24 (1996) 464S.
[30] R.S. Pitcher, N.J. Watmough, The bacterial cytochrome cbb_3 oxidases, Biochim. Biophys. Acta 1655 (2004) 388–399.
[31] V. Sharma, M. Wikström, L. Laakkonen, Modeling the active-site structure of the cbb_3-type oxidase from *Rhodobacter sphaeroides*, Biochemistry 47 (2008) 4221–4227.
[32] V. Sharma, M. Wikström, V.R.I. Kaila, Stabilization of the peroxy intermediate in the oxygen splitting reaction of cytochrome cbb_3, Biochim. Biophys. Acta 1807 (2011) 813–818.

[33] M. Toledo-Cuevas, B. Barquera, R.B. Gennis, M. Wikström, J.A. García-Horsman, The cbb_3-type cytochrome *c* oxidase from *Rhodobacter sphaeroides*, a proton-pumping heme-copper oxidase, Biochim. Biophys. Acta 1365 (1998) 421–434.
[34] S. Tsukita, S. Koyanagi, K. Nagata, H. Koizuka, H. Akashi, T. Shimoyama, T. Tamura, N. Sone, Characterization of a *cb*-type cytochrome *c* oxidase from *Helicobacter pylori*, J. Biochem. 125 (1999) 194–201.
[35] E. Arslan, A. Kannt, L. Thöny-Meyer, H. Hennecke, The symbiotically essential cbb_3-type oxidase of *Bradyrhizobium japonicum* is a proton pump, FEBS Lett. 470 (2000) 7–10.
[36] A.A. Konstantinov, S. Siletsky, D. Mitchell, A. Kaulen, R.B. Gennis, The roles of two proton input channels in cytochrome *c* oxidase from *Rhodobacter sphaeroides* probed by the effects of site-directed mutations on time-resolved electrogenic intraprotein proton transfer, Proc. Natl. Acad. Sci. U. S. A. 94 (1997) 9085–9090.
[37] D. Bloch, I. Belevich, A. Jasaitis, C. Ribacka, A. Puustinen, M.I. Verkhovsky, M. Wikström, The catalytic cycle of cytochrome *c* oxidase is not the sum of its two halves, Proc. Natl. Acad. Sci. U. S. A. 101 (2004) 529–533.
[38] H. Chang, J. Hemp, Y. Chen, J.A. Fee, R.B. Gennis, The cytochrome ba_3 oxygen reductase from *Thermus thermophilus* uses a single input channel for proton delivery to the active site and for proton pumping, Proc. Natl. Acad. Sci. U. S. A. 106 (2009) 16169–16173.
[39] A.D. Becke, Density-functional exchange-energy approximation with correct asymptotic behaviour, Phys. Rev. A 38 (1988) 3098–3100.
[40] J.P. Perdew, Density-functional approximation for the correlation energy of the inhomogeneous electron gas, Phys. Rev. B 33 (1986) 8822–8824.
[41] M. Sierka, A. Hogekamp, R. Ahlrichs, Fast evaluation of the coulomb potential for electron densities using multipole accelerated resolution of identity approximation, J. Chem. Phys. 118 (2003) 9136–9148.
[42] R. Ahlrichs, M. Bär, M. Häser, H. Horn, C. Kölmel, Electronic structure calculations on workstation computers: the program system turbomole, Chem. Phys. Lett. 162 (1989) 165–169.
[43] A. Schäfer, H. Horn, R. Ahlrichs, Fully optimized contracted Gaussian basis sets for atoms Li to Kr, J. Chem. Phys. 97 (1992) 2571–2577.
[44] F. Weigend, R. Ahlrichs, Balanced basis sets of split valence, triple zeta valence and quadruple zeta valence quality for H to Rn: design and assessment of accuracy, Phys. Chem. Chem. Phys. 7 (2005) 3297–3305.
[45] A.D. Becke, Density-functional thermochemistry. III. The role of exact exchange, J. Chem. Phys. 98 (1993) 5648–5652.
[46] C. Lee, W. Yang, R.G. Parr, Development of the Colle-Salvetti correlation-energy formula into a functional of the electron density, Phys. Rev. B 37 (1988) 785–789.
[47] U.C. Singh, P.A. Kollman, An approach to computing electrostatic charges for molecules, J. Comp. Chem. 5 (1984) 129–145.
[48] A. Klamt, G. Schüürmann, COSMO: a new approach to dielectric screening in solvents with explicit expressions for the screening energy and its gradient, J. Chem. Soc. Perkin Trans. 2 (1993) 799–805.
[49] M.P. Johansson, V.R.I. Kaila, L. Laakkonen, Charge parameterization of the metal centers in cytochrome *c* oxidase, J. Comp. Chem. 29 (2008) 753–767.
[50] K. Nilsson, H.P. Hersleth, T.H. Rod, K.K. Andersson, U. Ryde, The protonation status of compound II in myoglobin, studied by a combination of experimental data and quantum chemical calculations: quantum refinement, Biophys. J. 87 (2004) 3437–3447.
[51] G.M. Ullmann, L. Noodleman, D.A. Case, Density functional calculation of pK_a values and redox potentials in the bovine Rieske iron–sulfur protein, J. Biol. Inorg. Chem. 7 (2002) 632–639.
[52] M. Compoint, C. Ramseyer, P. Huetz, Ab initio investigation of the atomic charges in the KcsA channel selectivity filter, Chem. Phys. Lett. 397 (2004) 510–515.
[53] S. Izrailev, A.R. Crofts, E.A. Berry, K. Schulten, Steered molecular dynamics simulation of the Rieske subunit motion in the cytochrome bc_1 complex, Biophys. J. 77 (1999) 1753–1768.
[54] L. Zhang, J. Hermans, Hydrophilicity of cavities in proteins, Proteins: Struct. Funct. Genet. 24 (1996) 433–438.
[55] I. Hofacker, K. Schulten, Oxygen and proton pathways in cytochrome *c* oxidase, Proteins: Struct. Funct. Genet. 30 (1998) 100–107.
[56] X. Zheng, D.M. Medvedev, J. Swanson, A.A. Stuchebrukhov, Computer simulation of water in cytochrome *c* oxidase, Biochim. Biophys. Acta 1557 (2003) 99–107.
[57] S.A. Seibold, D.A. Mills, S. Ferguson-Miller, R.I. Cukier, Water chain formation and possible proton pumping routes in *Rhodobacter sphaeroides* cytochrome *c* oxidase: a molecular dynamics comparison of the wild type and R481K mutant, Biochemistry 44 (2005) 10475–10485.
[58] R.I. Cukier, A molecular dynamics study of water chain formation in the proton-conducting K channel of cytochrome *c* oxidase, Biochim. Biophys. Acta 1706 (2005) 134–146.
[59] E. Olkhova, M.C. Hutter, M.A. Lill, V. Helms, H. Michel, Dynamic water networks in cytochrome C oxidase from *Paracoccus denitrificans* investigated by molecular dynamics simulations, Biophys. J. 86 (2004) 1873–1889.
[60] J.C. Rasaiah, S. Garde, G. Hummer, Water in nonpolar confinement: from nanotubes to proteins and beyond, Annu. Rev. Phys. Chem. 59 (2008) 713–740.
[61] A.D. MacKerell Jr., D. Bashford, M. Bellott, R.L. Dunbrack Jr., J.D. Evanseck, M.J. Field, S. Fischer, J. Gao, H. Guo, S. Ha, et al., All-atom empirical potential for molecular modeling and dynamics studies of proteins, J. Phys. Chem. B 102 (1998) 3586–3616.
[62] F. Autenrieth, E. Tajkhorshid, J. Baudry, Z. Luthey-Schulten, Classical force field parameters for the heme prosthetic group of cytochrome *c*, J. Comp. Chem. 25 (2004) 1613–1622.
[63] J.C. Phillips, R. Braun, W. Wang, J. Gumbart, E. Tajkhorshid, E. Villa, C. Chipot, R.D. Skeel, L. Kale, K. Schulten, Scalable molecular dynamics with NAMD, J. Comp. Chem. 26 (2005) 1781–1802.
[64] W. Humphrey, A. Dalke, K. Schulten, VMD — Visual Molecular Dynamics, J. Mol. Graph. 14 (1996) 33–38.
[65] D. Bashford, K. Gerwert, Electrostatic calculations of the pK_a values of ionizable groups in bacteriorhodopsin, J. Mol. Biol. 224 (1992) 473–486.
[66] D. Bashford, An object-oriented programming suite for electrostatic effects in biological molecules, in: Y. Ishikawa, R.R. Oldehoeft, J.V.W. Reynders, M. Tholburn (Eds.), Scientific Computing in Object-oriented Parallel Environments, Springer, Berlin/Heidelberg, 1997, pp. 233–240.
[67] Y. Song, E. Michonova-Alexova, M.R. Gunner, Calculated proton uptake on anaerobic reduction of cytochrome *c* oxidase: is the reaction electroneutral? Biochemistry 45 (2006) 7959–7975.
[68] W.L. Jorgensen, J. Chandrasekhar, J.D. Madura, R.W. Impey, M.L. Klein, Comparison of simple potential functions for simulating liquid water, J. Chem. Phys. 79 (1983) 926–935.
[69] B. Rabenstein, E.W. Knapp, Calculated pH-dependent population and protonation of carbon-monoxy-myoglobin conformers, Biophys. J. 80 (2001) 1141–1150.
[70] P.J. Goodford, A computational procedure for determining energetically favorable binding sites on biologically important macromolecules, J. Med. Chem. 28 (1985) 849–857.
[71] S. Riistama, G. Hummer, A. Puustinen, R.B. Dyer, W.H. Woodruff, M. Wikström, Bound water in the proton translocation mechanism of the haem-copper oxidases, FEBS Lett. 414 (1997) 275–280.
[72] V.R.I. Kaila, G. Hummer, Energetics and dynamics of proton transfer reactions along short water wires, Phys. Chem. Chem. Phys. 13 (2011) 13207–13215.
[73] G. Hummer, J.C. Rasaiah, J.P. Noworyta, Water conduction through the hydrophobic channel of a carbon nanotube, Nature 414 (2001) 188–190.
[74] M. Wikström, M.I. Verkhovsky, G. Hummer, Water-gated mechanism of proton translocation by cytochrome c oxidase, Biochim. Biophys. Acta 1604 (2003) 61–65.
[75] D.B. Goodin, D.E. McRee, The Asp-His-iron triad of cytochrome *c* peroxidase controls the reduction potential electronic structure, and coupling of the tryptophan free radical to the heme, Biochemistry 32 (1993) 3313–3324.
[76] T. Soulimane, G. Buse, G.P. Bourenkov, H.D. Bartunik, R. Huber, M.E. Than, Structure and mechanism of the aberrant ba_3-cytochrome *c* oxidase from *Thermus thermophilus*, EMBO J. 19 (2000) 1766–1776.
[77] V. Daskalakis, S.C. Farantos, V. Guallar, C. Varotsis, Regulation of electron and proton transfer by the protein matrix of cytochrome *c* oxidase, J. Phys. Chem. B. 115 (2011) 3648–3655.
[78] A. Kannt, C.R.D. Lancaster, H. Michel, The coupling of electron transfer and proton translocation: electrostatic calculations on *Paracoccus denitrificans* cytochrome *c* oxidase, Biophys. J. 74 (1998) 708–721.
[79] R. Zufferey, E. Arslan, L. Thöny-Meyer, H. Hennecke, How replacement of the 12 conserved histidines of subunit I affect assembly, cofactor binding, and enzymatic activity of the *Bradyrhizobium japonicum* cbb_3-type oxidase, J. Biol. Chem. 273 (1998) 6452–6459.
[80] J.I. Oh, Effect of mutation of five conserved histidine residues in the catalytic subunit of the cbb_3 cytochrome *c* oxidase on its function, J. Microbiol. 44 (2006) 284–292.
[81] R.M. Henry, C.H. Yu, T. Rodinger, R. Pomès, Functional hydration and conformational gating of proton uptake in cytochrome *c* oxidase, J. Mol. Biol. 387 (2009) 1165–1185.
[82] V.R.I. Kaila, M.I. Verkhovsky, G. Hummer, M. Wikström, Glutamic acid 242 is a valve in the proton pump of cytochrome *c* oxidase, Proc. Natl. Acad. Sci. U. S. A. 105 (2008) 6255–6259.
[83] V.R.I. Kaila, M.I. Verkhovsky, G. Hummer, M. Wikström, Mechanism and energetics by which glutamic acid 242 prevents leaks in cytochrome *c* oxidase, Biochim. Biophys. Acta 1787 (2009) 1205–1214.
[84] M. Wikström, K. Krab, M. Saraste, Cytochrome Oxidase: A Synthesis, Academic Press, London, 1981.
[85] M. Özturk, E. Gurel, N.J. Watmough, S. Mandaci, Site-directed mutagenesis of five conserved residues in subunit I of the cytochrome cbb_3 oxidase in *Rhodobacter capsulatus*, J. Biochem. Mol. Biol. 40 (2007) 697–707.
[86] I. Belevich, E. Gorbikova, N.P. Belevich, V. Rauhamäki, M. Wikström, M.I. Verkhovsky, Initiation of the proton pump of cytochrome *c* oxidase, Proc. Natl. Acad. Sci. U. S. A. 107 (2010) 18469–18474.